Atomic data
(Fe XIII density diagnostics for Hinode EIS)

Giulio Del Zanna
DAMTP, CMS, University of Cambridge, UK

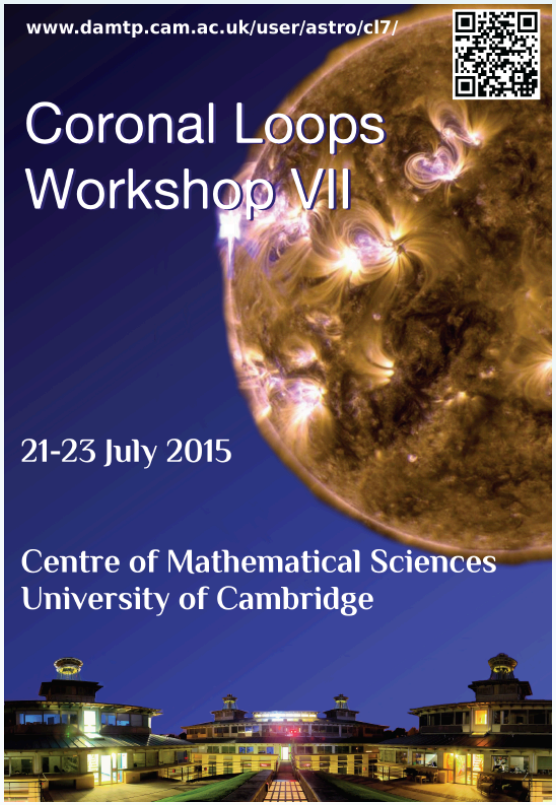

Science & Technology Facilities Council

SEVENTH FRAMEWORK PROGRAMME

solid

UNIVERSITY OF CAMBRIDGE

Atomic data

SPECTROSCOPY OF STELLAR CORONAE:

Measurements of Ne, Te, DEM(T), flows

CALCULATION:

UK **APAP Network** http://www.apap-network.org/
has become the main ion atomic data provider
for fusion and astrophysics
(Strathclyde, UCL, Cambridge)

BENCHMARK:

EUV line identifications and benchmark

DISTRIBUTION:

CHIANTI (www.chiantidatabase.org) has now become the reference atomic database for ions

CHIANTI v.7 are available in VAMDC (Virtual Atomic and Molecular Data Center: http://portal.vamdc.eu)

Ionization vs. excitation

Ionizations/recombinations occur on timescales of 1-100s

Dipole-allowed lines decay in 10^{-10} s. Forbidden ones in 10^{-4} s or longer

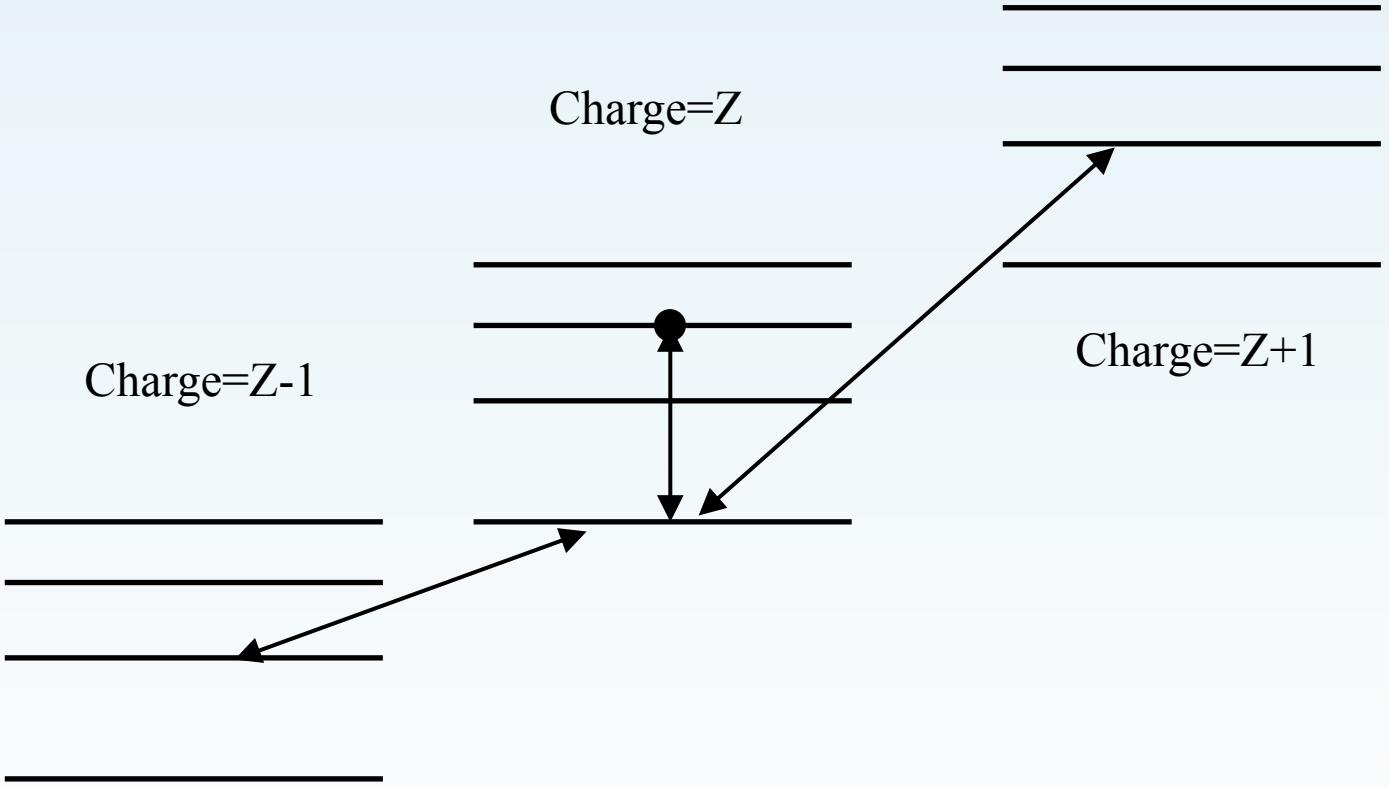

Normally consider separately excitation / ionization

Line intensities

In optically-thin plasmas line intensities are proportional to:

$$I \sim n_j \, A_{ji} = \frac{N_j(X^{+m})}{N(X^{+m})} \, A_{ji} \, \frac{N(X^{+m})}{N(X)} \, \frac{N(X)}{N(H)} \frac{N(H)}{N_e} \, N_e$$

Level population (Ne,Te)

A-value

Ion abundance (Te, Ne)

El. abundance

The Hydrogen/electron density depends on the elemental abundances relative to H. For the solar corona, H, He are fully ionised and the ratio is about 0.8--0.9.

Contribution function

Spectral line intensity:

$$I(\lambda_{ij}) = \frac{h\nu_{ij}}{4\pi} \int N_j \, A_{ji} \, dh \; = \int Ab(X) C(T, \lambda_{ij}, N_e) N_e N_H dh \quad [\text{ergs cm}^{-2} \text{ s}^{-1} \text{ sr}^{-1}]$$

$$C(T, \lambda_{ij}, N_e) = \frac{h\nu_{ij}}{4\pi} \frac{A_{ji}}{N_e} \frac{N_j(X^{+m})}{N(X^{+m})} \frac{N(X^{+m})}{N(X)} \quad [\text{ergs cm}^{+3} \text{ s}^{-1}]$$

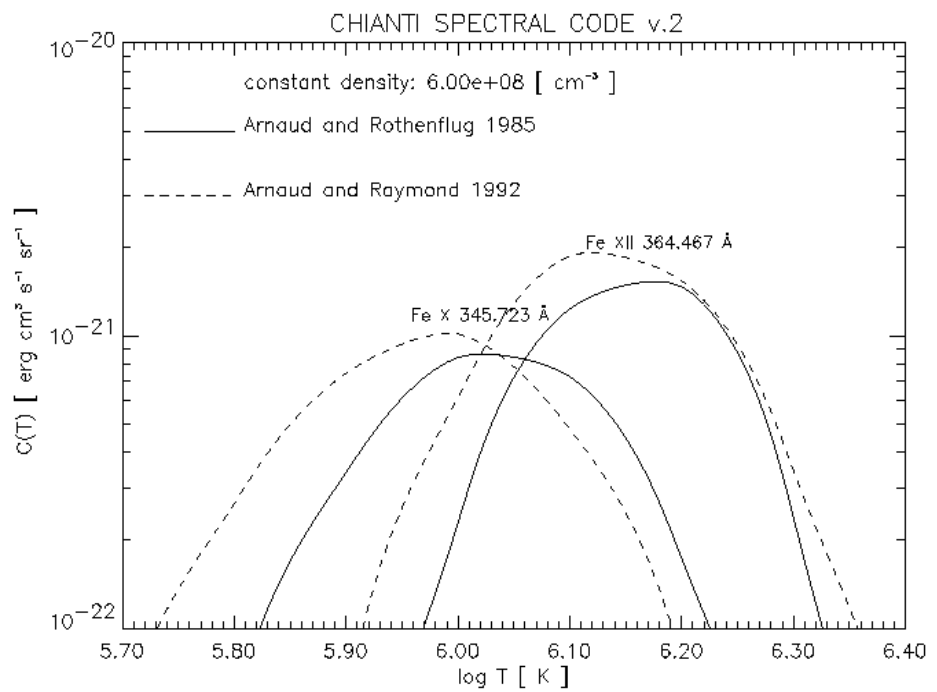

Level population

The main processes affecting the level populations are scattering with particles and photons.

All excitations/de-excitations need to be considered.

$$\frac{dN_{\rm j}}{dt} = \sum_{i>j} N_i \mathcal{A}_{ij} + \sum_{i>j} N_i N_{\rm e} C^{\rm e}_{ij} + \sum_{i<j} N_i N_{\rm e} C^{\rm e}_{ij} + \sum_{i>j} N_i N_{\rm p} C^{\rm p}_{ij} + \sum_{i<j} N_i N_{\rm p} C^{\rm p}_{ij} - N_j \Big(\sum_{i<j} \mathcal{A}_{ji} + N_{\rm e} \sum_{i<j} C^{\rm e}_{ji} + N_{\rm e} \sum_{i>j} C^{\rm e}_{ji} + N_{\rm p} \sum_{i<j} C^{\rm p}_{ji} + N_{\rm p} \sum_{i>j} C^{\rm p}_{ji} \Big)$$

Most abundant particles in the quiescent corona are thermal electrons, protons, alpha.

Electron collisions are the main excitation process in the low corona.

Proton collisions are also important for some ions.

Non-thermal particles could be present.

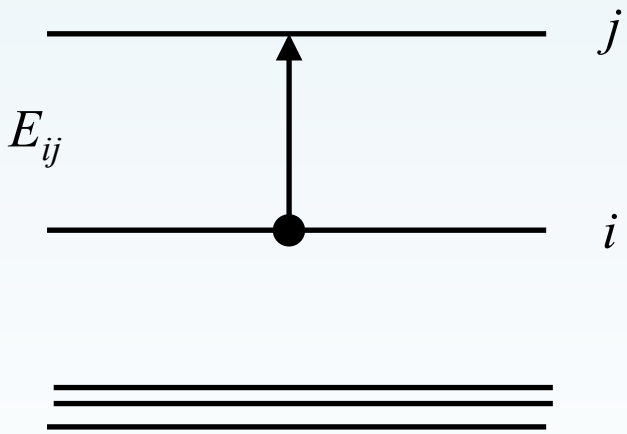

Collision strength

The number of transitions form level i to level j due to electron collisions per unit volume and time is given by Ni Ne Cij where Cij is the rate:

$$C^e_{ij} = \int_{v_o}^{\infty} v\sigma_{ij}(v) f(v) dv$$

collision strength

$$\sigma_{ij} = \frac{\pi a_0^2}{g_i} \frac{E_H}{E} \Omega_{ij}(E)$$

Assuming a Maxwellian distribution function *f*:

$$C^e_{ij} = 8.63\ 10^{-6} \frac{\Upsilon_{ij}}{T_e^{1/2} g_i}\ exp\left(-\frac{E_{ij}}{kT_e}\right)$$

$$\Upsilon_{ij} = \int_0^{\infty} \Omega_{ij}\ exp\left(-\frac{E_j}{kT_e}\right) d\left(\frac{E_j}{kT_e}\right)$$

Collision strength- example: Mg IX

intercombination

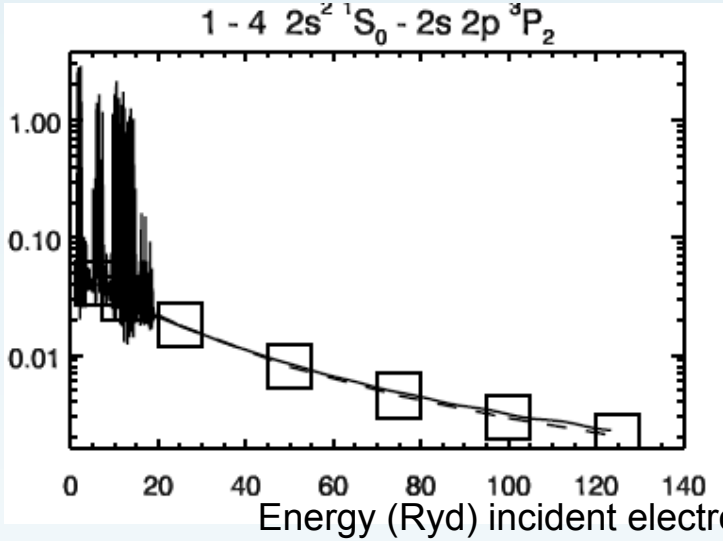

allowed

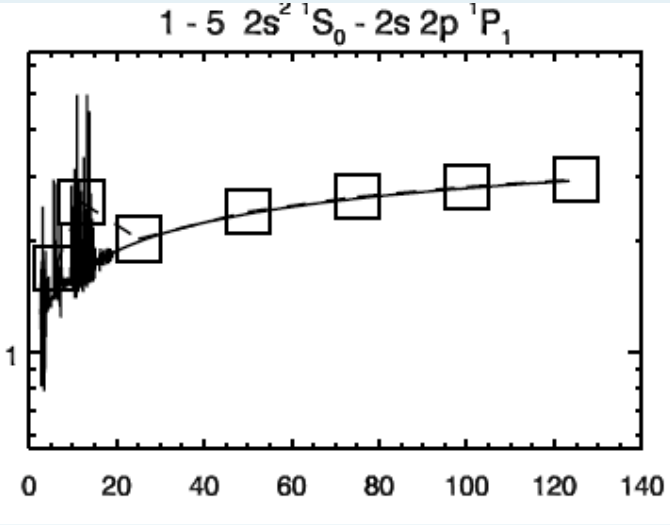

Energy (Ryd) incident electron

Coll. strength

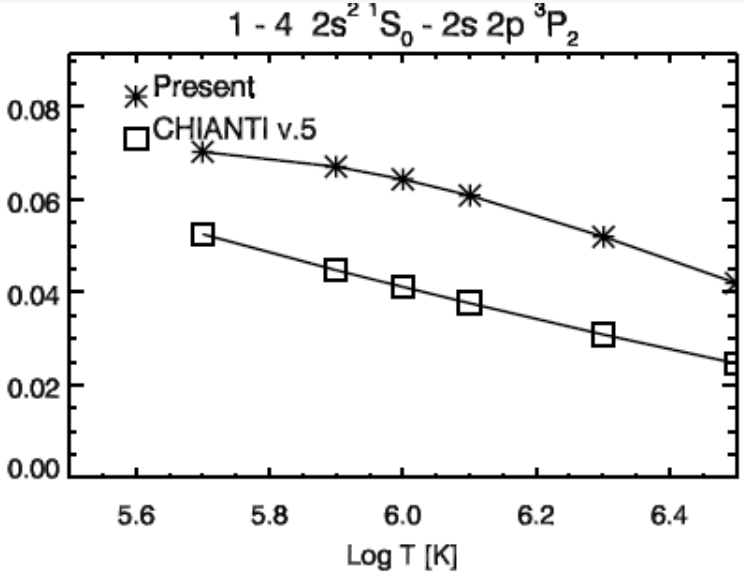

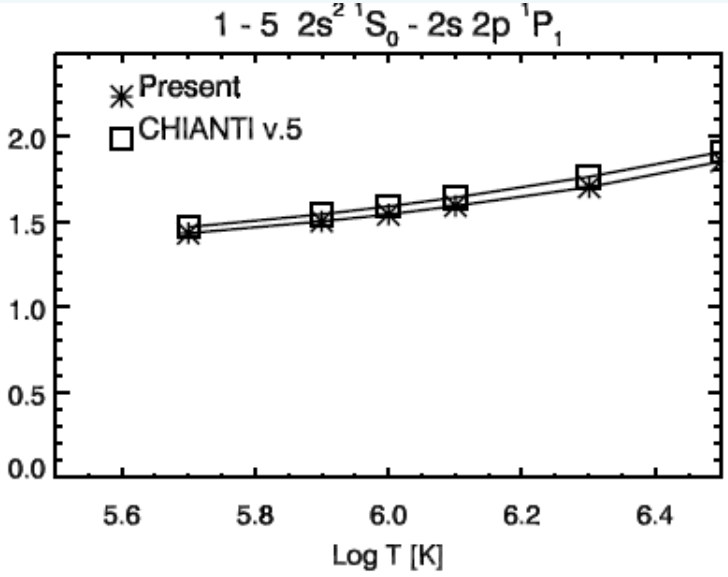

Maxwellian avg. Coll. strength

Del Zanna et al. (2008)

Metastable levels- electron density diagnostics

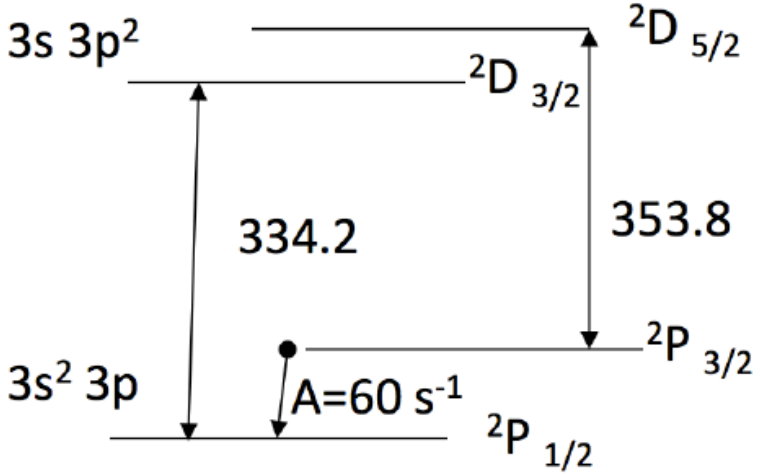

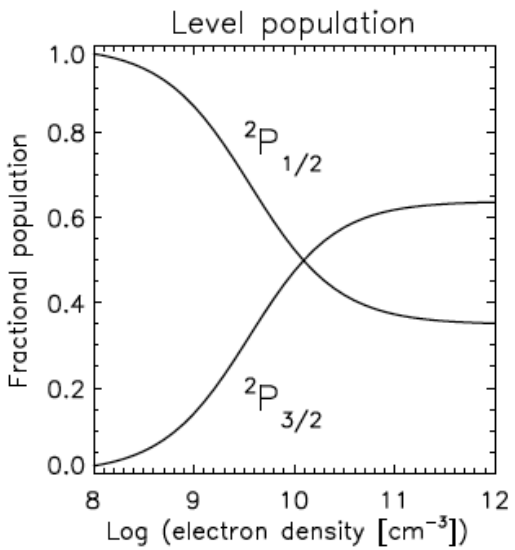

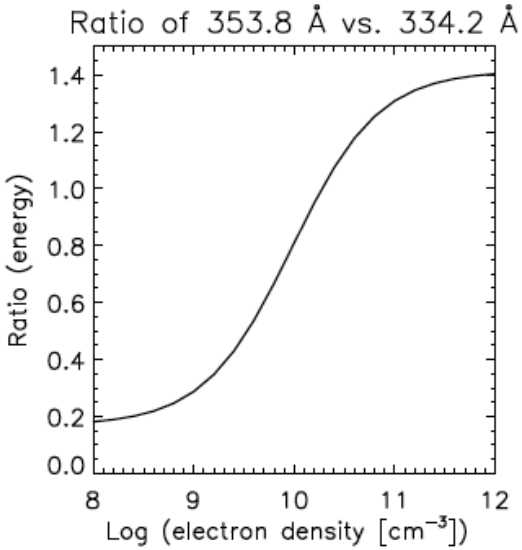

As the electron density increases, the population of the metastable levels increases.

The intensity of spectral lines connected with metastable levels varies accordingly.

The CHIANTI IDL program to measure densities from line ratios

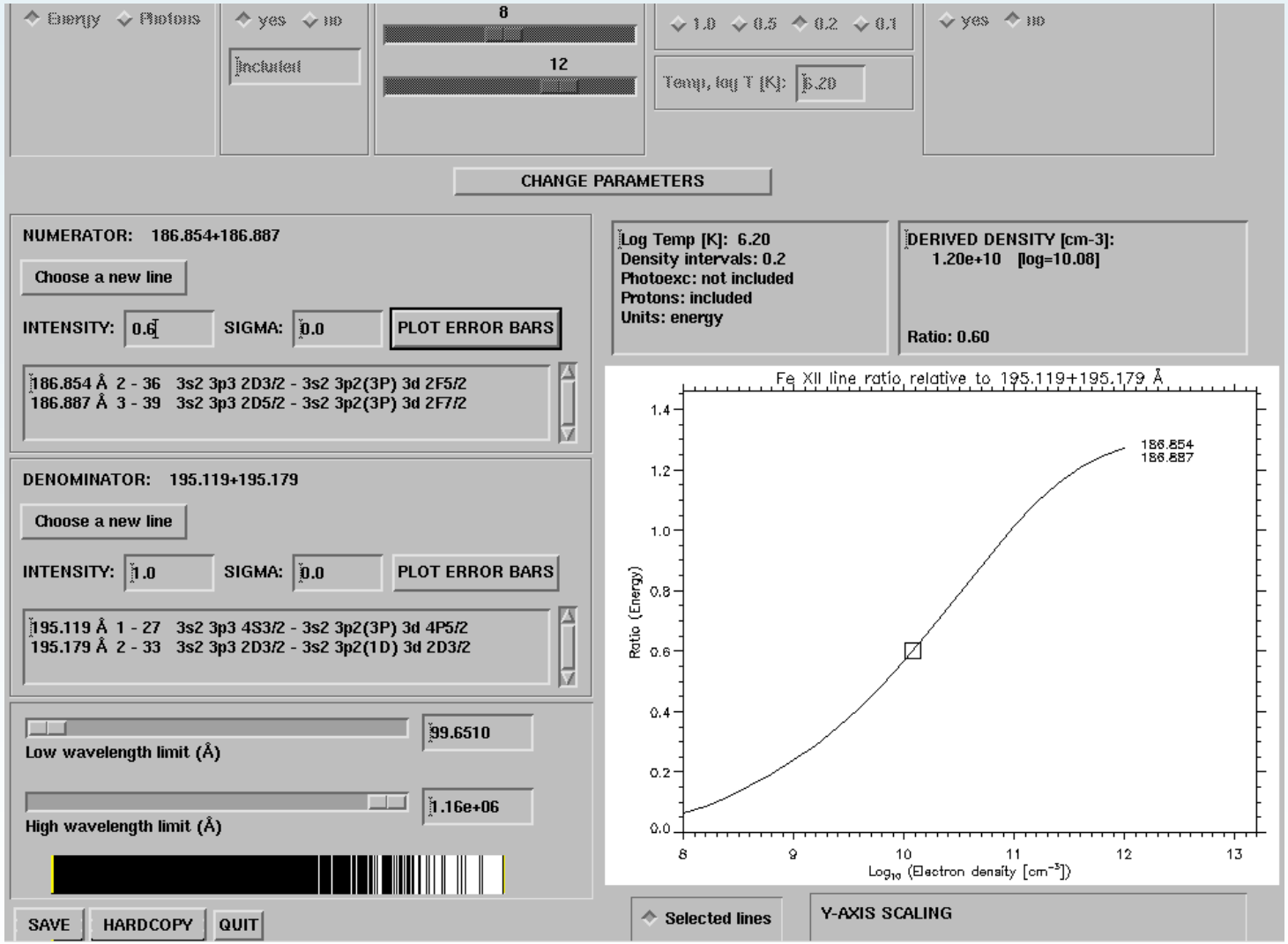

Hinode EUV imaging spectrometer (EIS)

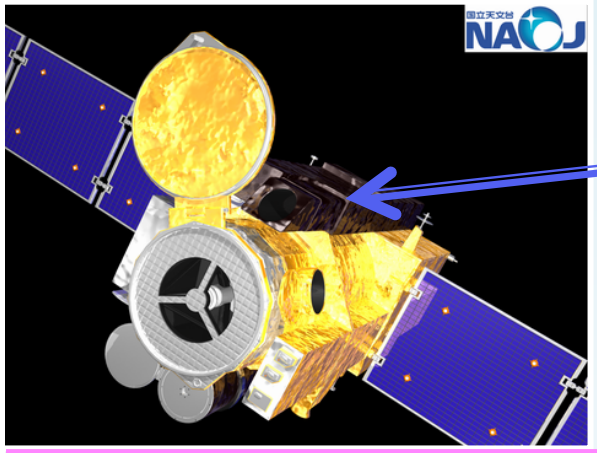

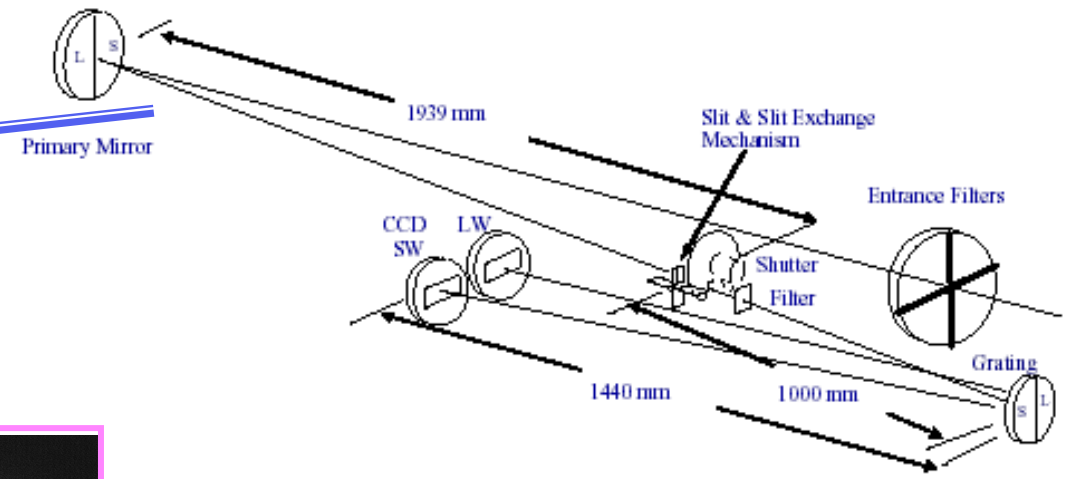

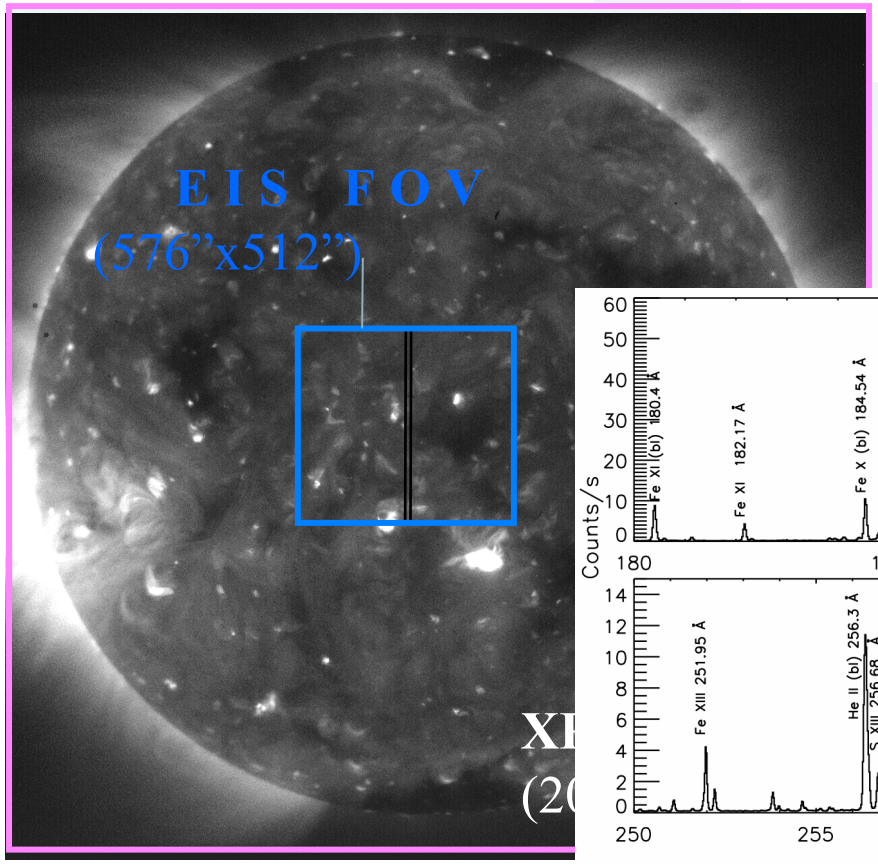

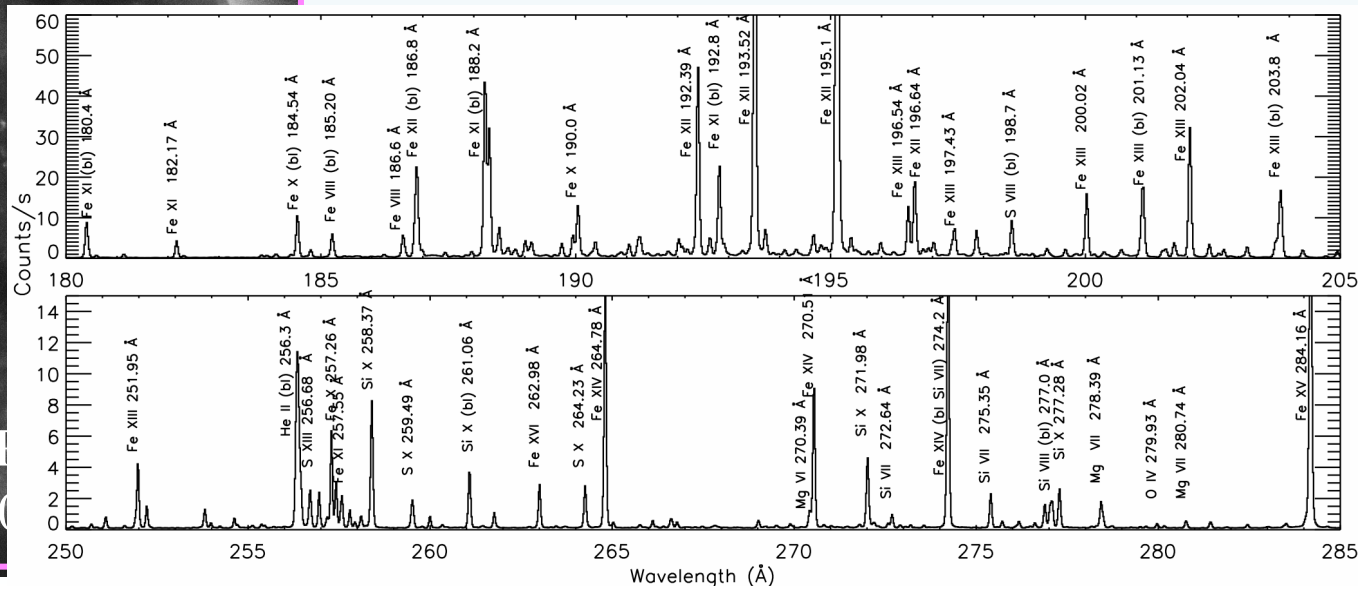

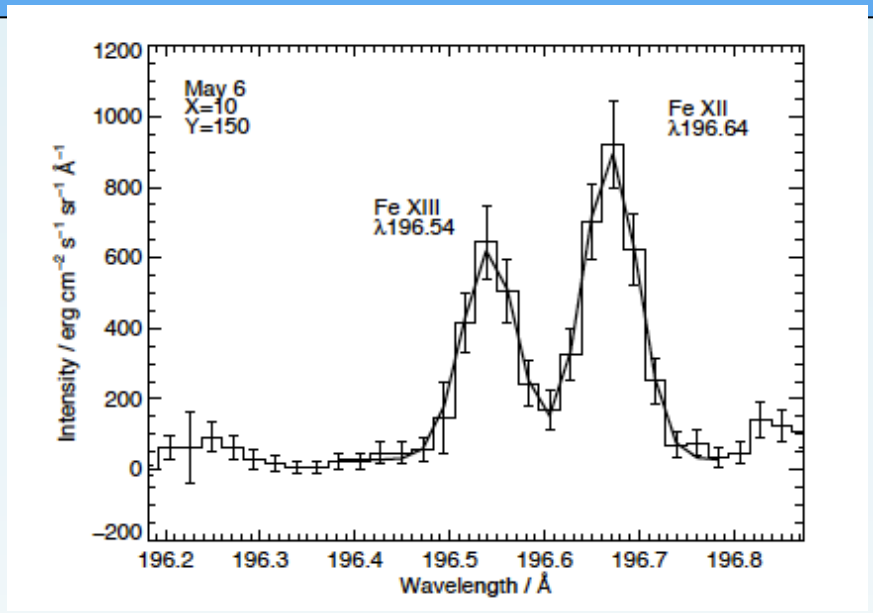

Hinode EIS
Young et al. (2008)

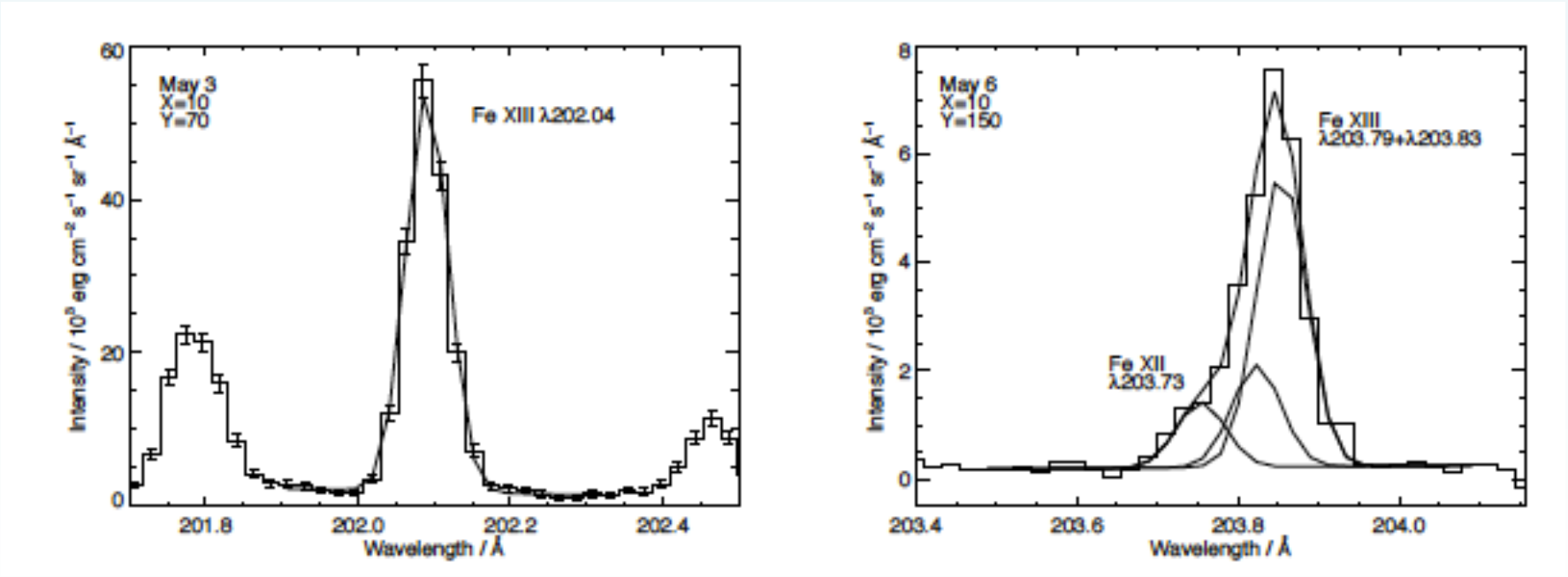

Young et al. 2008

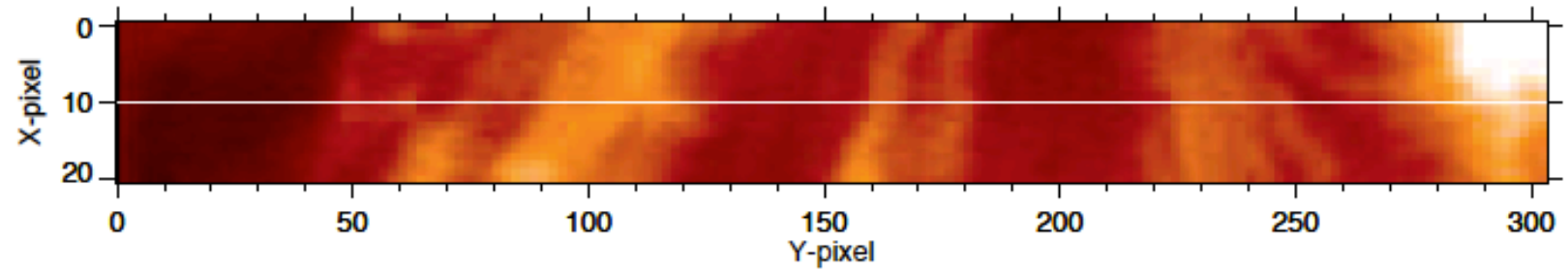

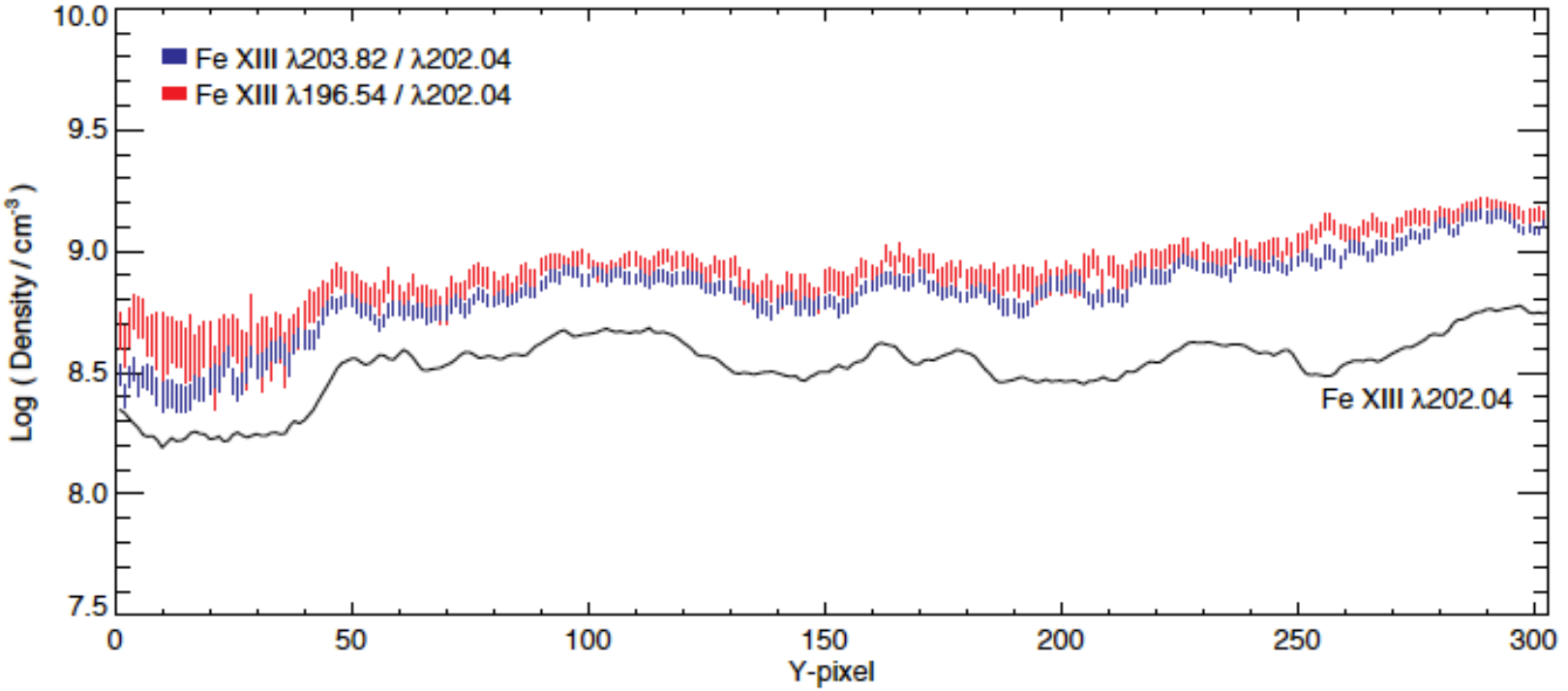

Used older collision strengths from Gupta & Tayal (1998)

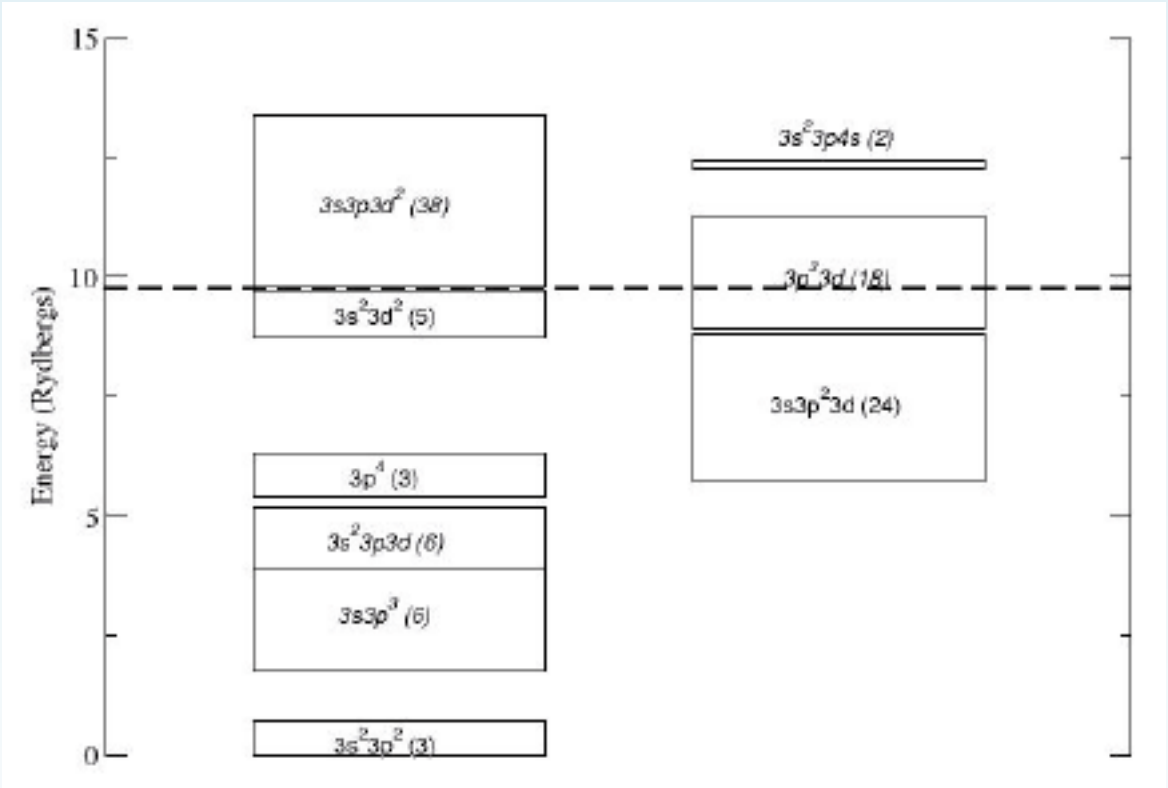

Storey & Zeippen (2010) performed an IP scattering calculation much superior than previous ones.

Benchmarking atomic data (Del Zanna)

1) observed and theoretical wavelengths and line intensities for a wide range of astrophysical and laboratory plasmas using the emissivity ratios:

$$F_{ji}(N_e, T_e) = C \frac{I_{ob} N_e}{N_j(N_e, T_e) A_{ji}}$$

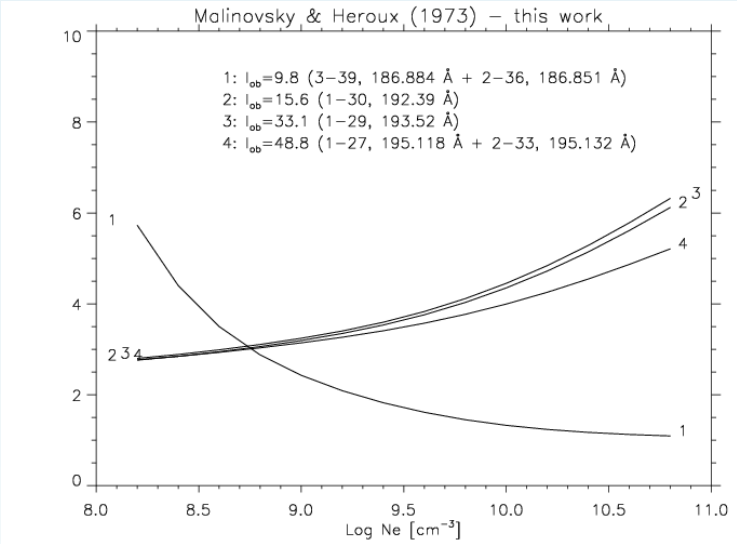

Storey et al.(2005)

For iso-density plasmas, curves cross.

The method in principle could be used to infer the density distribution alos. (Doschek (1984)
But.. large uncertainties in atomic data and calibration!

2) compared level lifetimes with beam-foil spectroscopy.
RESULTS:
new wavelengths (with uncertainties), new identifications, new level energies (with uncertainties), new diagnostics

A-values of strongest lines normally accurate to better than 10%
Excitation data can be accurate to better than 20%

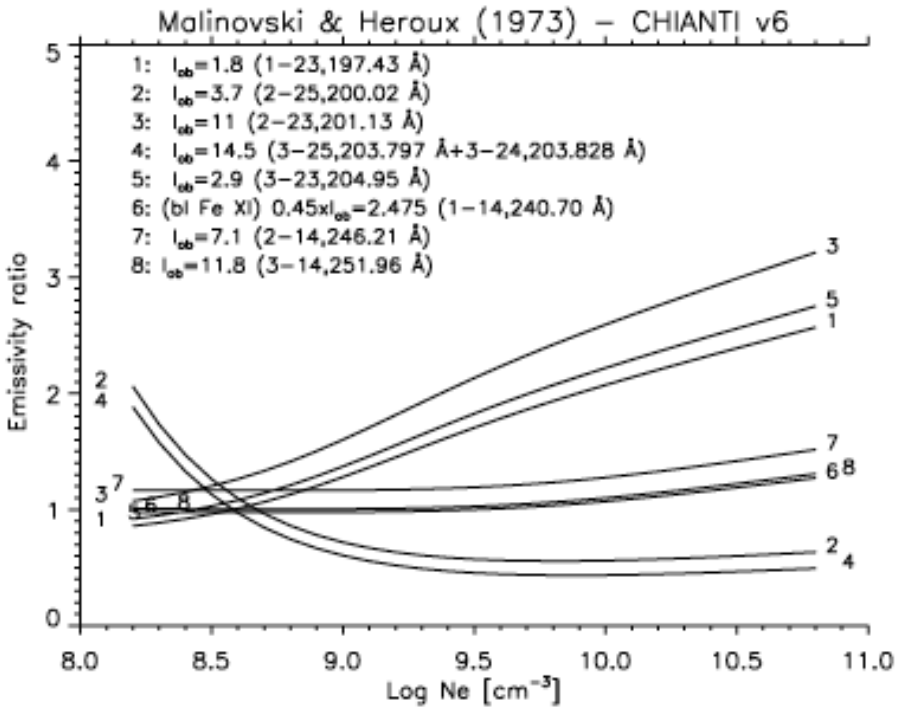

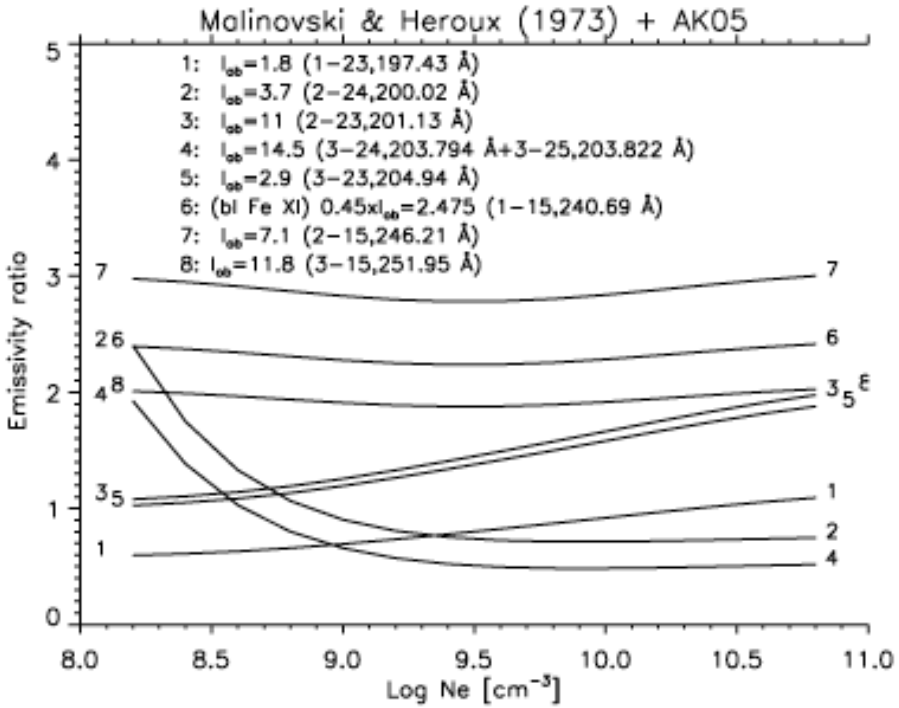

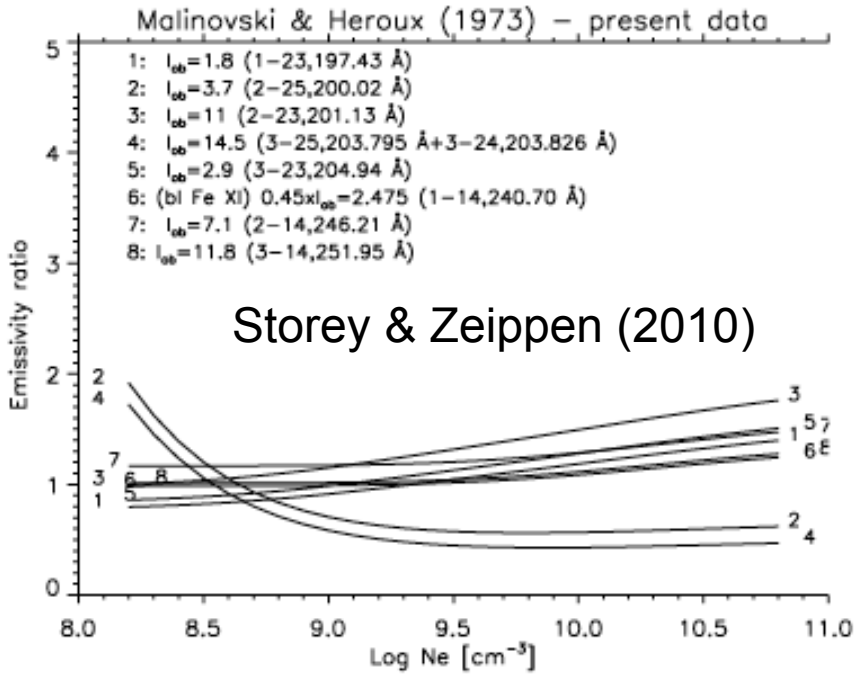

Storey & Zeippen (2010)

Large problems with atomic data of Aggarwal & Keenan 2005.

Gupta & Tayal (1998) – CHIANTI v6

(learn who to trust!)

Del Zanna A&A 533, A12 (2011)

Table 1. Level energies for Fe XIII.

i	Conf.	Lev.	E_{exp}	E_{NIST}
1	$3s^2\ 3p^2$	$^3P_0$	0.0	0.0 (0)
2	$3s^2\ 3p^2$	$^3P_1$	9303.1	9302.5 (1)
3	$3s^2\ 3p^2$	$^3P_2$	18 561.7	18 561.0 (1)
4	$3s^2\ 3p^2$	$^1D_2$	48 069.7	48 068.0 (2)
5	$3s^2\ 3p^2$	$^1S_0$	91 511.0	91 508.0 (3)
6	$3s\ 3p^3$	$^5S_2$	214 624.0	214 608.0 (16)
7	$3s\ 3p^3$	$^3D_1$	287 205.0	287 205.0 (0)
8	$3s\ 3p^3$	$^3D_2$	287 356.0	287 360.0 (–4)
9	$3s\ 3p^3$	$^3D_3$	290 180.0	290 210.0 (–30)
10	$3s\ 3p^3$	$^3P_0$	328 927.0	–
11	$3s\ 3p^3$	$^3P_1$	329 637.0	329 647.0 (–10)
12	$3s\ 3p^3$	$^3P_2$	330 282.0	330 279.0 (3)
13	$3s\ 3p^3$	$^1D_2$	362 407.0	362 330.0 (77)
14	$3s\ 3p^3$	$^3S_1$	415 462.0	415 462.0 (0)
15	$3s^2\ 3p\ 3d$	$^3F_2$	430 124.0	–
16	$3s\ 3p^3$	$^1P_1$	438 086.0	438 050.0 (36)
17	$3s^2\ 3p\ 3d$	$^3F_3$	436 919.0	–
18	$3s^2\ 3p\ 3d$	$^3F_4$	447 001.0	–
19	$3s^2\ 3p\ 3d$	$^3P_2$	486 358.0	486 358.0 (0)
20	$3s^2\ 3p\ 3d$	$^3P_1$	494 942.0	494 942.0 (0)
21	$3s^2\ 3p\ 3d$	$^1D_2$	498 870.0	498 870.0 (0)
22	$3s^2\ 3p\ 3d$	$^3P_0$	501 514.0	503 340.0 (–1826)
23	$3s^2\ 3p\ 3d$	$^3D_1$	506 505.0	506 502.0 (3)
24	$3s^2\ 3p\ 3d$	$^3D_3$	509 176.0	509 176.0 (0)
25	$3s^2\ 3p\ 3d$	$^3D_2$	509 250.0	509 250.0 (0)
26	$3s^2\ 3p\ 3d$	$^1F_3$	556 911.0	556 870.0 (41)
27	$3s^2\ 3p\ 3d$	$^1P_1$	570 743.0	570 690.0 (53)
28	$3p^4$	$^3P_2$	591 362.0	–
42	$3s\ 3p^2\ 3d$	$^3F_2$	669 564.0	–
56	$3s\ 3p^2\ 3d$	$^3D_2$	753 767.0	–
60	$3s\ 3p^2\ 3d$	$^3F_2$	777 950.0	–
61	$3s\ 3p^2\ 3d$	$^3F_3$	783 540.0	–
64	$3s\ 3p^2\ 3d$	$^3F_4$	792 105.0	–
72	$3s\ 3p^2\ 3d$	$^3D_2$	817 170.0	–
84	$3s\ 3p^2\ 3d$	$^3P_2$	897 511.0	–

Several new identifications, to be confirmed !

Del Zanna A&A 533, A12 (2011)

Table 2. List of the brightest Fe XIII lines, from the EUV to the visible.

$i-j$	Int 1×10^{8}	Int 1×10^{12}	λ_{exp} (Å)	λ_{NIST} (Å)	
1–20	1.0	0.12	202.044	202.044	
3–14	0.26	0.19	251.952	251.952	
2–23	0.20	0.10	201.126	201.127	
3–20	0.15	1.8×10^{-2}	209.916	209.916	
2–14	0.13	9.8×10^{-2}	246.209	246.209	
3–24	7.4×10^{-2}	0.39	203.826	203.826	sbl
3–23	6.3×10^{-2}	3.2×10^{-2}	204.942	204.943	
1–14	5.4×10^{-2}	3.9×10^{-2}	240.696	240.696	bl
1–23	4.0×10^{-2}	2.1×10^{-2}	197.431	197.433	
3–25	3.4×10^{-2}	0.14	203.795	203.795	sbl
7–60	3.0×10^{-2}	4.3×10^{-3}	203.772	–	N sbl
3–17	3.3×10^{-2}	3.4×10^{-2}	239.030	–	N
4–16	3.6×10^{-2}	0.13	256.400	256.422	R bl
2–25	2.4×10^{-2}	9.9×10^{-2}	200.021	200.021	
4–15	2.7×10^{-2}	1.4×10^{-2}	261.743	–	N
4–21	2.1×10^{-2}	0.15	221.828	221.827	
2–19	1.8×10^{-2}	8.6×10^{-2}	209.619	209.619	
8–60	1.8×10^{-2}	2.5×10^{-3}	203.835	–	N sbl

Several new identifications

Del Zanna A&A 533, A12 (2011)

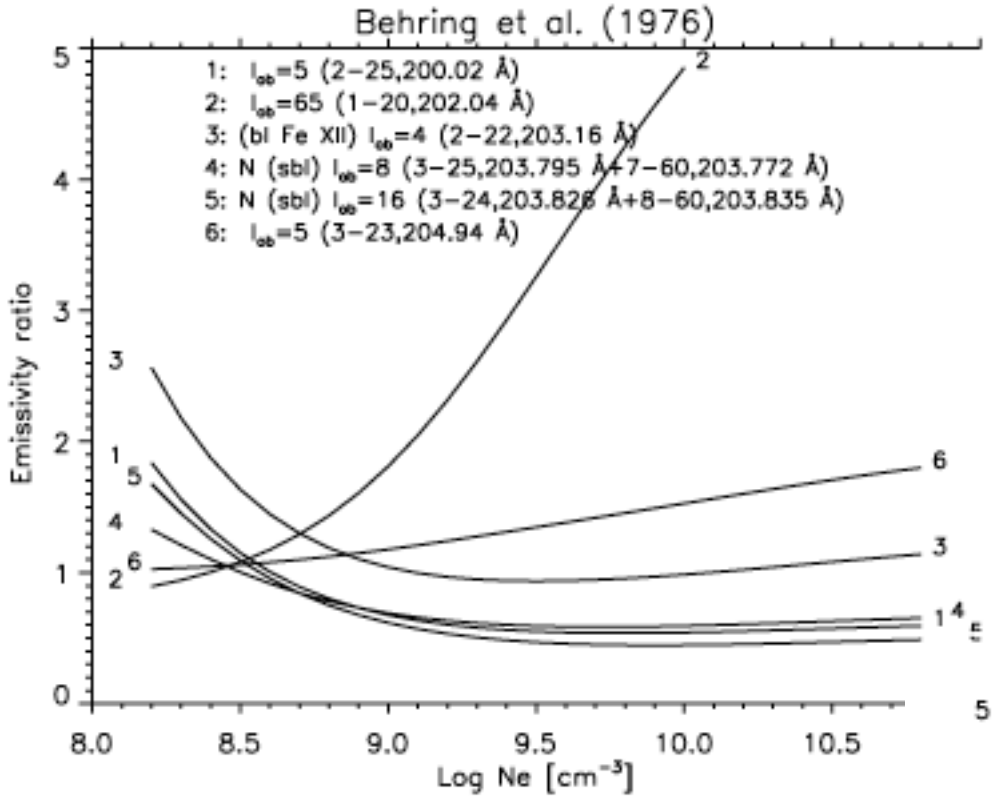

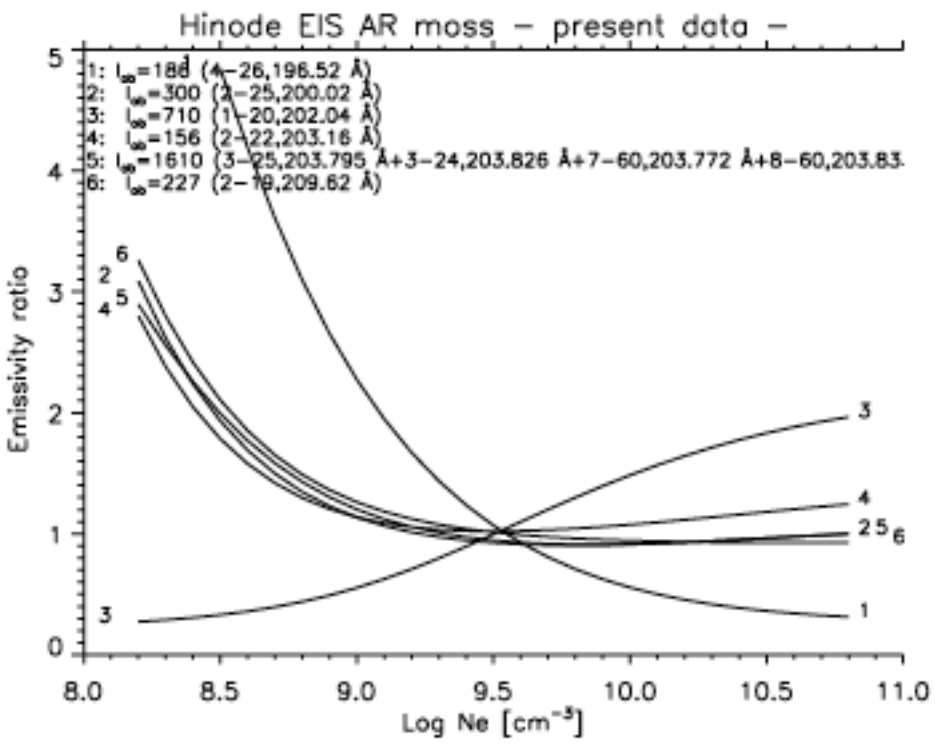

High-resolution observations seem to confirm the new identifications

Del Zanna A&A 533, A12 (2011)

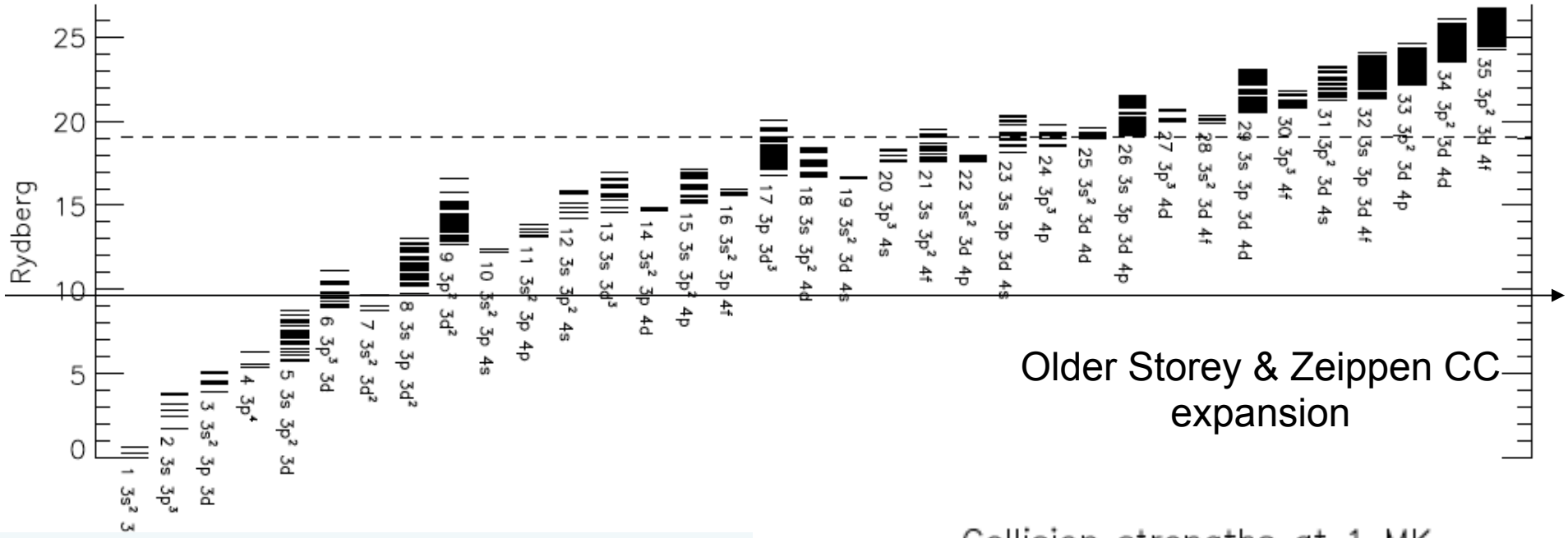

Older Storey & Zeippen CC expansion

Del Zanna & Storey (2012): largest scattering calculation to date → CHIANTI v.8 (Del Zanna+2015). Only minor differences for strongest lines, compared to Storey & Zeippen (2010).

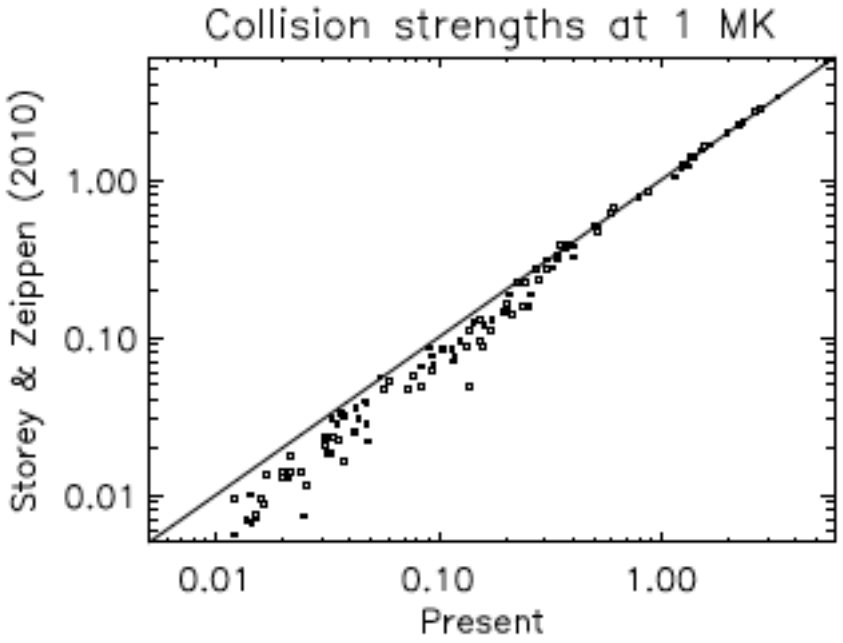

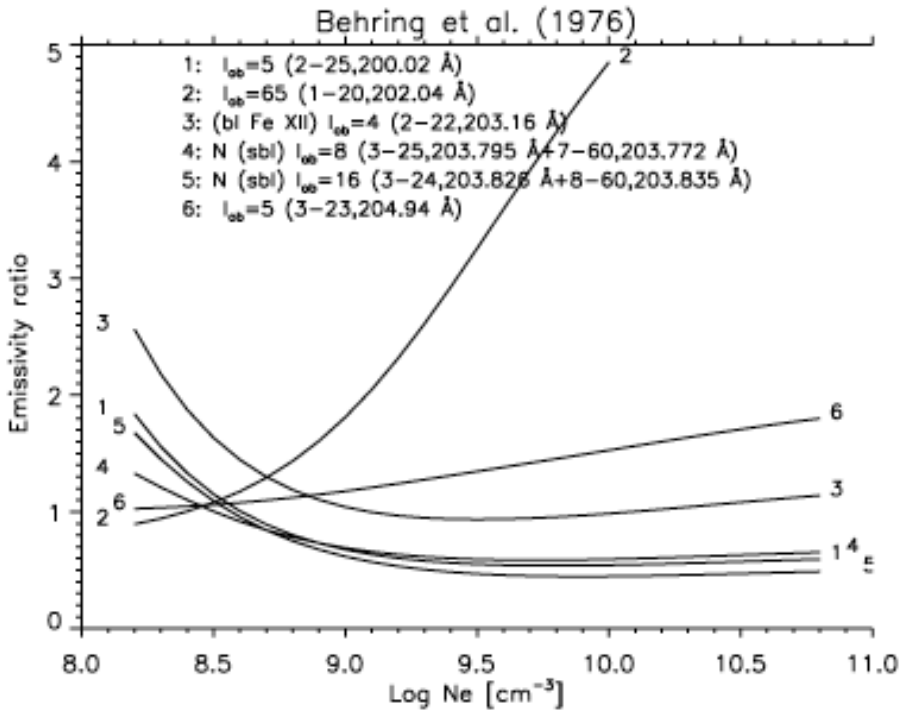
Behring et al. (1976)
1: I_{ob}=5 (2–25,200.02 Å)
2: I_{ob}=65 (1–20,202.04 Å)
3: (bl Fe XII) I_{ob}=4 (2–22,203.16 Å)
4: N (sbl) I_{ob}=8 (3–25,203.795 Å+7–60,203.772 Å)
5: N (sbl) I_{ob}=16 (3–24,203.826 Å+8–60,203.835 Å)
6: I_{ob}=5 (3–23,204.94 Å)
Emissivity ratio
Log Ne [cm^{-3}]

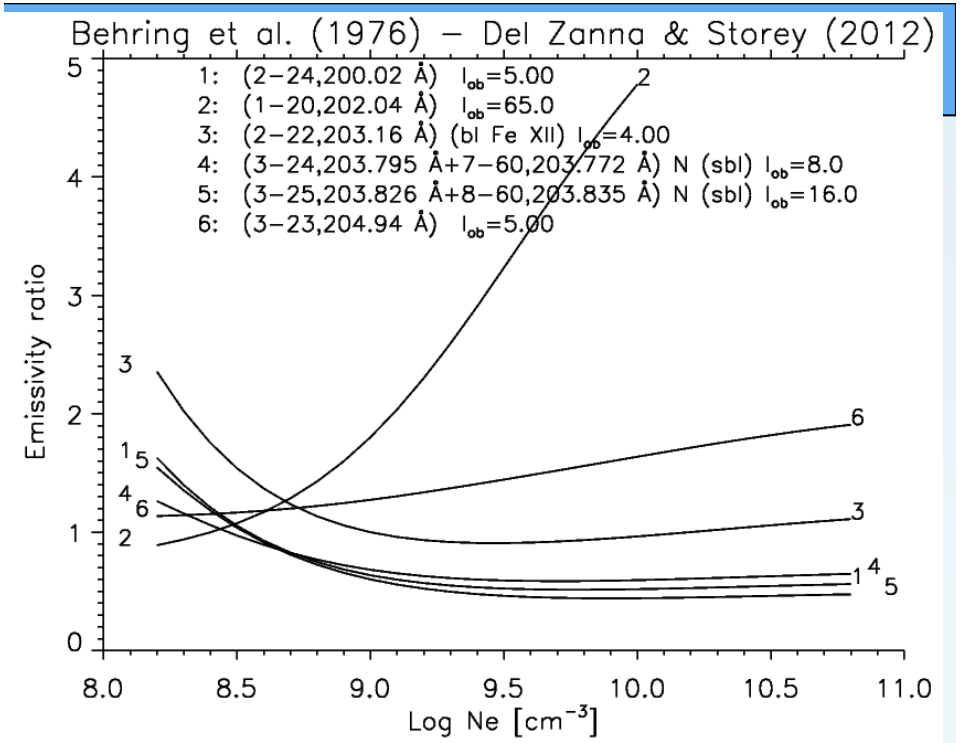
Behring et al. (1976) – Del Zanna & Storey (2012)
1: (2–24,200.02 Å) I_{ob}=5.00
2: (1–20,202.04 Å) I_{ob}=65.0
3: (2–22,203.16 Å) (bl Fe XII) I_{ob}=4.00
4: (3–24,203.795 Å+7–60,203.772 Å) N (sbl) I_{ob}=8.0
5: (3–25,203.826 Å+8–60,203.835 Å) N (sbl) I_{ob}=16.0
6: (3–23,204.94 Å) I_{ob}=5.00
Emissivity ratio
Log Ne [cm^{-3}]

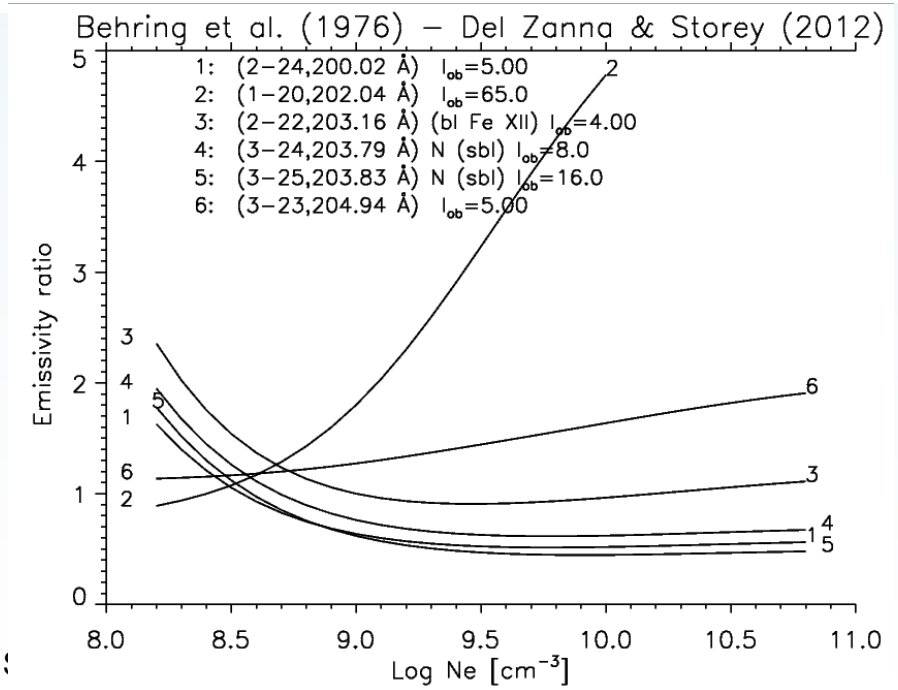
Behring et al. (1976) – Del Zanna & Storey (2012)
1: (2–24,200.02 Å) I_{ob}=5.00
2: (1–20,202.04 Å) I_{ob}=65.0
3: (2–22,203.16 Å) (bl Fe XII) I_{ob}=4.00
4: (3–24,203.79 Å) N (sbl) I_{ob}=8.0
5: (3–25,203.83 Å) N (sbl) I_{ob}=16.0
6: (3–23,204.94 Å) I_{ob}=5.00
Emissivity ratio
Log Ne [cm^{-3}]

Fe XIII – processes at 10^8 cm^{-3}

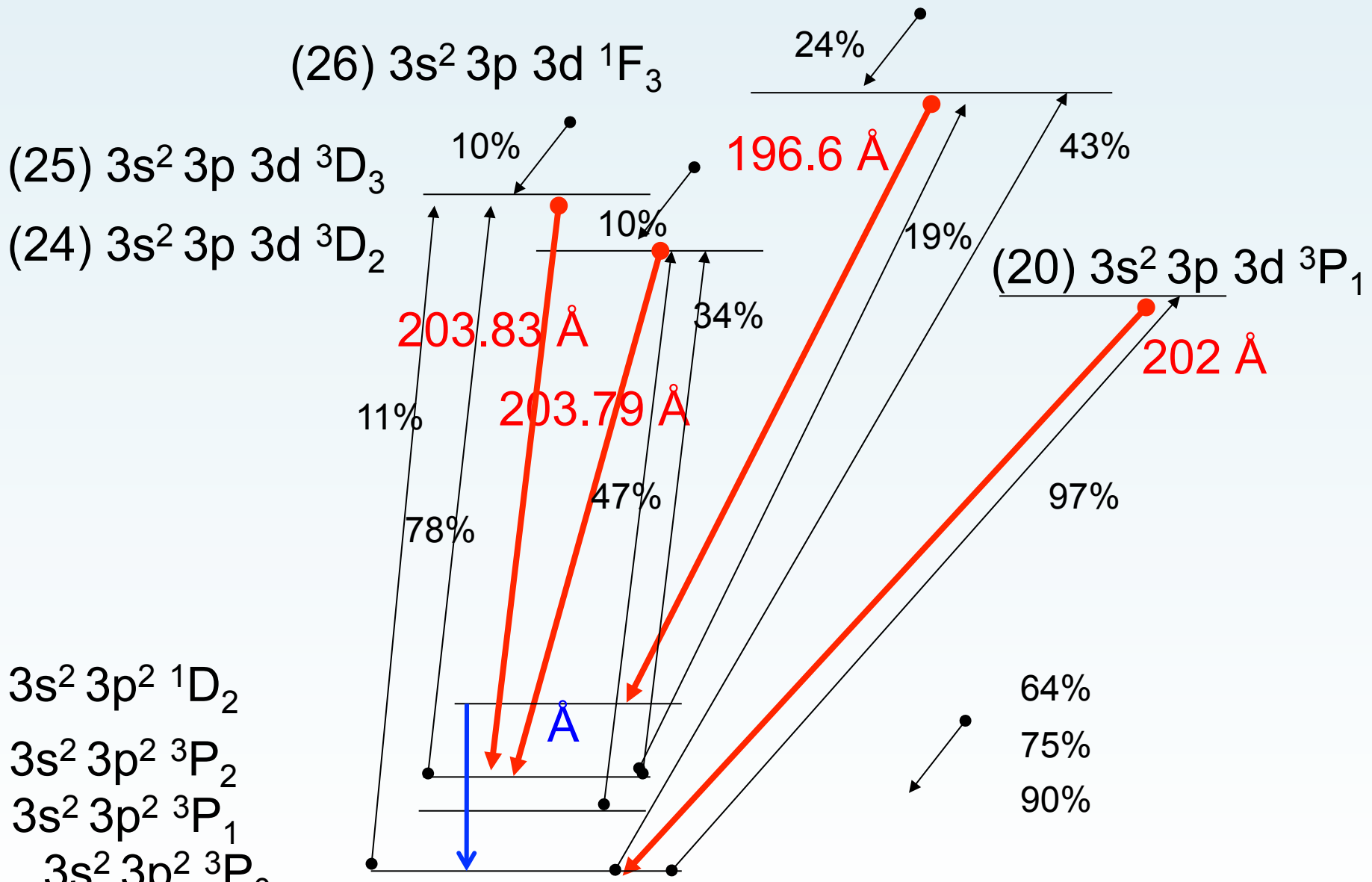

Del Zanna & Storey (2012)

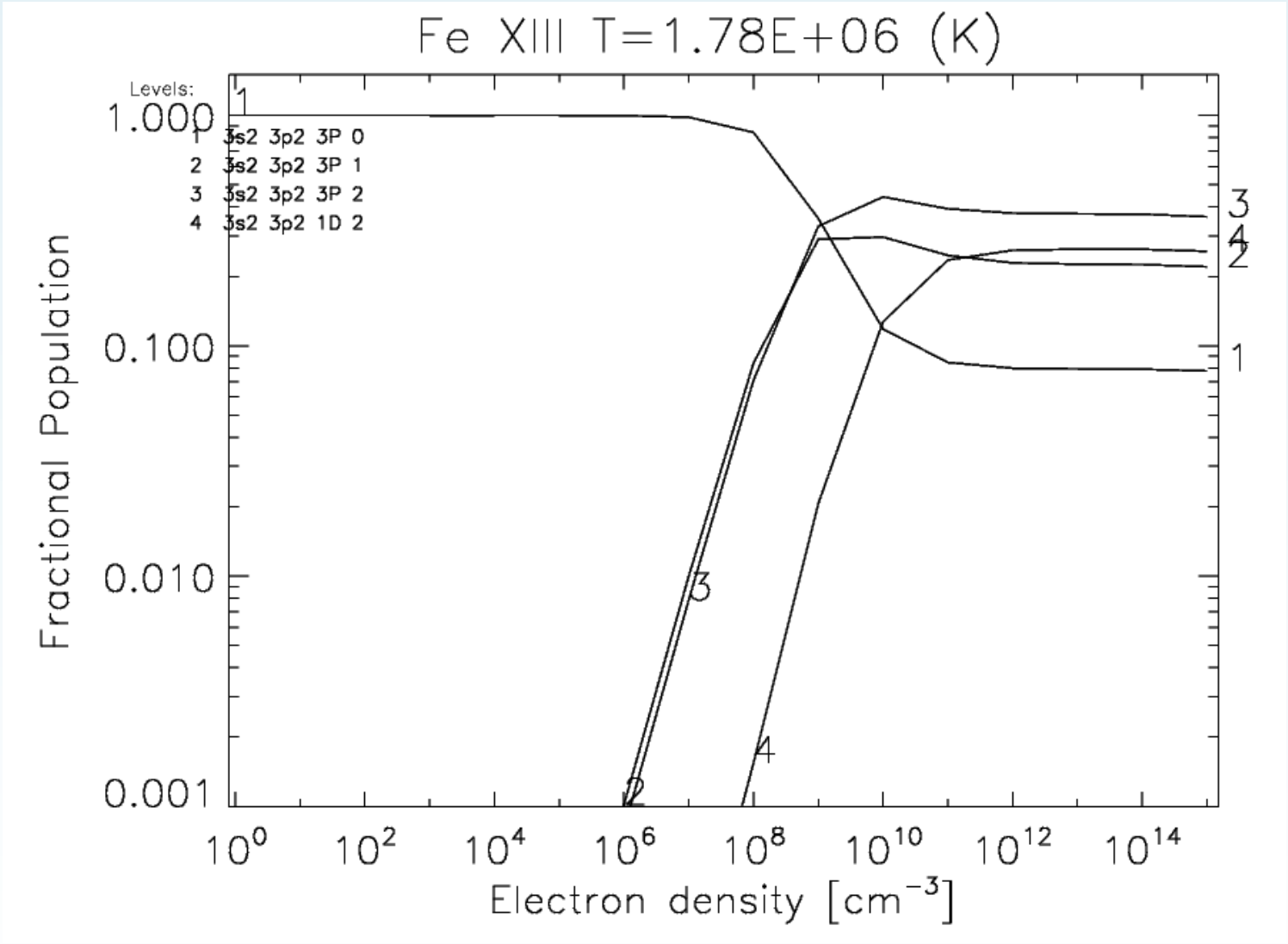
Fe XIII T=1.78E+06 (K)
Levels:
1 3s2 3p2 3P 0
2 3s2 3p2 3P 1
3 3s2 3p2 3P 2
4 3s2 3p2 1D 2
1.000
0.100
0.010
0.001
Fractional Population
10^0 10^2 10^4 10^6 10^8 10^{10} 10^{12} 10^{14}
Electron density [cm^{-3}]

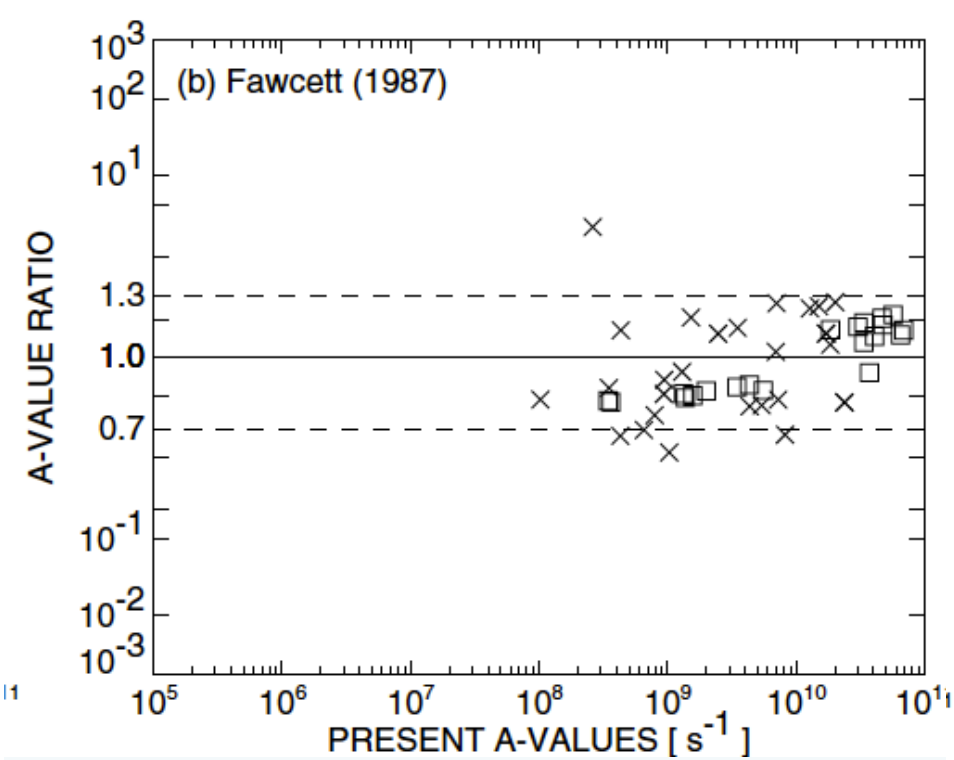

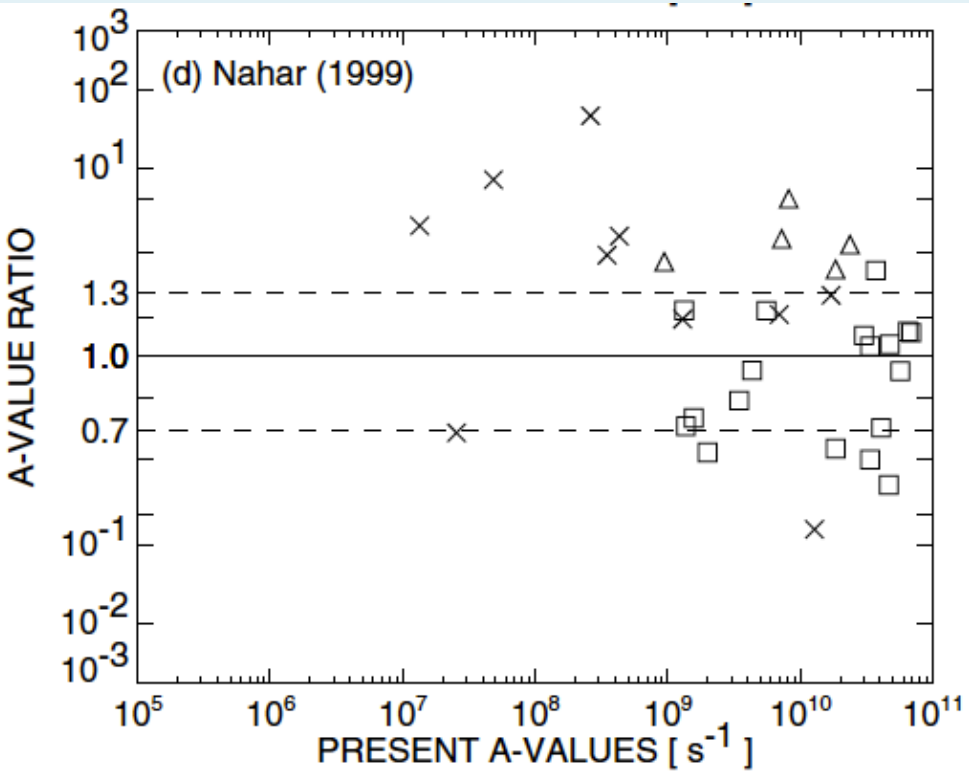

Young (2004) performed atomic structure calculations with TEC. In some case, large differences in the A-values of the strong allowed transitions are found (learn who to trust!).

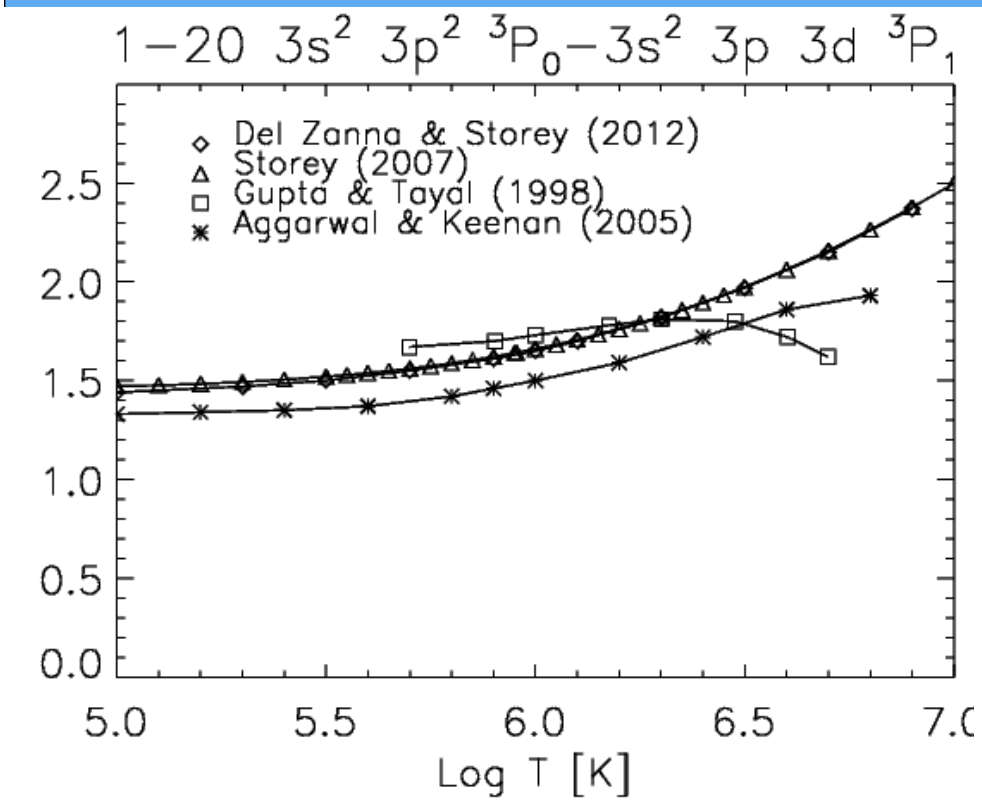
1−20 3s² 3p² ³P₀−3s² 3p 3d ³P₁
Del Zanna & Storey (2012)
Storey (2007)
Gupta & Tayal (1998)
Aggarwal & Keenan (2005)
2.5
2.0
1.5
1.0
0.5
0.0
5.0
5.5
6.0
6.5
7.0
Log T [K]

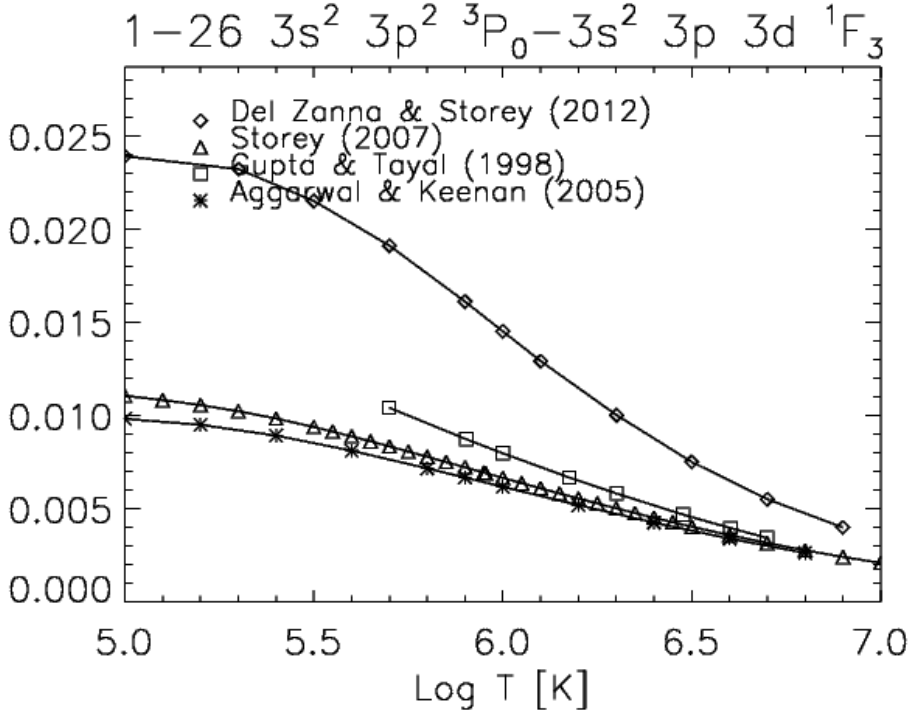
1−26 3s² 3p² ³P₀−3s² 3p 3d ¹F₃
Del Zanna & Storey (2012)
Storey (2007)
Gupta & Tayal (1998)
Aggarwal & Keenan (2005)
0.025
0.020
0.015
0.010
0.005
0.000
5.0
5.5
6.0
6.5
7.0
Log T [K]

Non-Maxwellian electrons

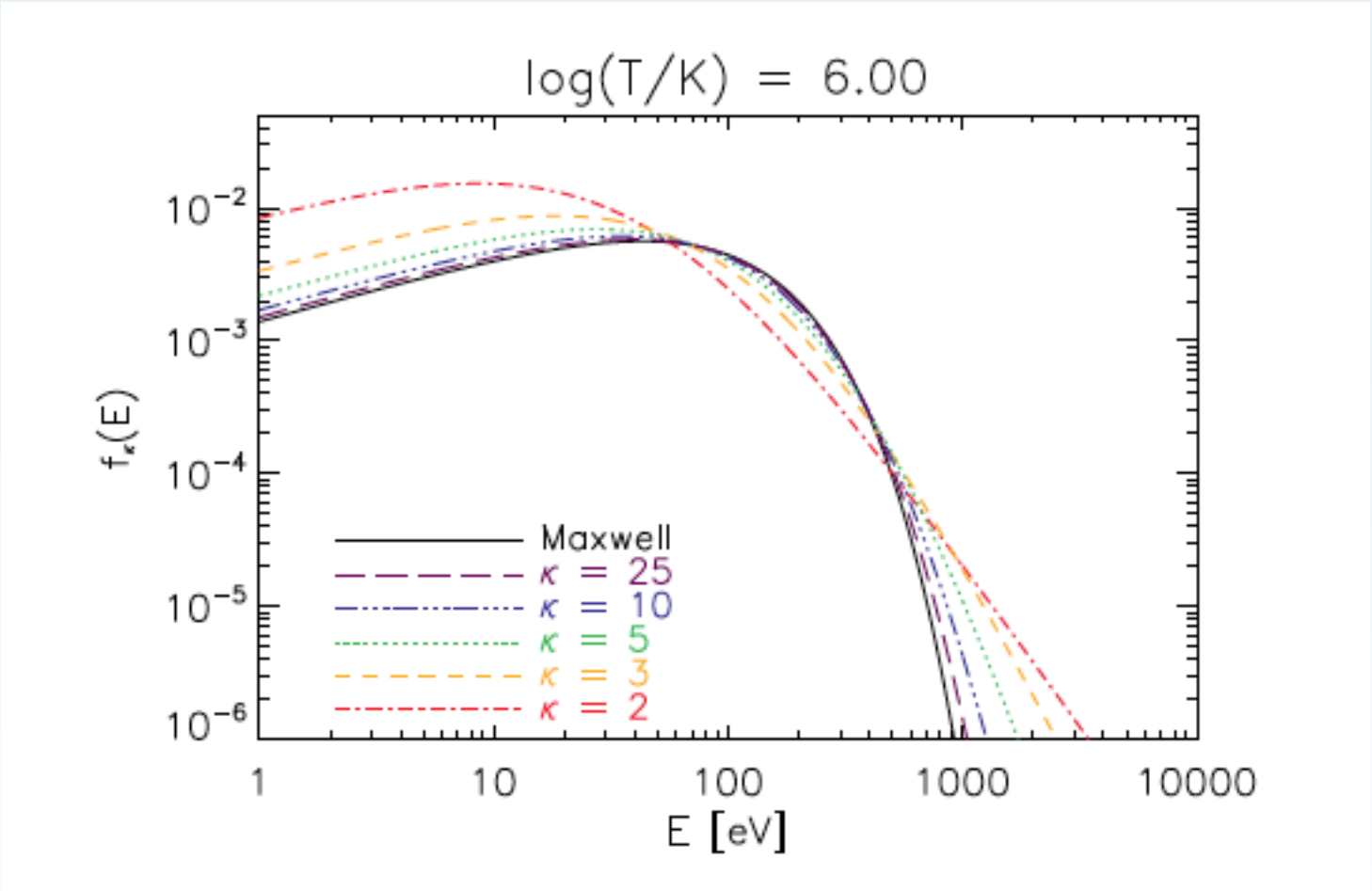

Dudik, Del Zanna et al. 2014, A&A

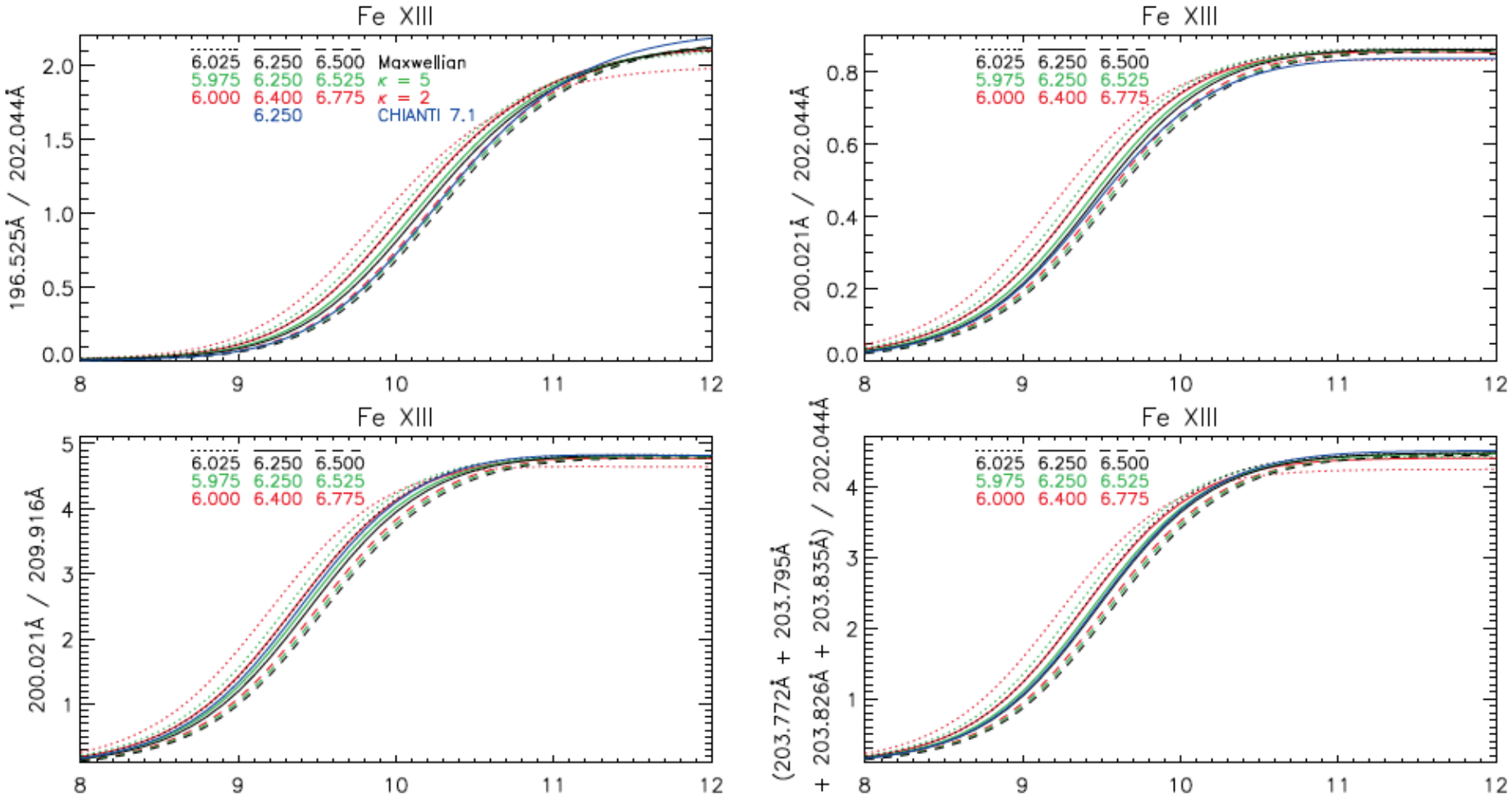
Fe XIII
196.525Å / 202.044Å
6.025 6.250 6.500 Maxwellian
5.975 6.250 6.525 κ = 5
6.000 6.400 6.775 κ = 2
6.250 CHIANTI 7.1
Fe XIII
200.021Å / 202.044Å
6.025 6.250 6.500
5.975 6.250 6.525
6.000 6.400 6.775
Fe XIII
200.021Å / 209.916Å
6.025 6.250 6.500
5.975 6.250 6.525
6.000 6.400 6.775
Fe XIII
(203.772Å + 203.795Å
+ 203.826Å + 203.835Å) / 202.044Å
6.025 6.250 6.500
5.975 6.250 6.525
6.000 6.400 6.775

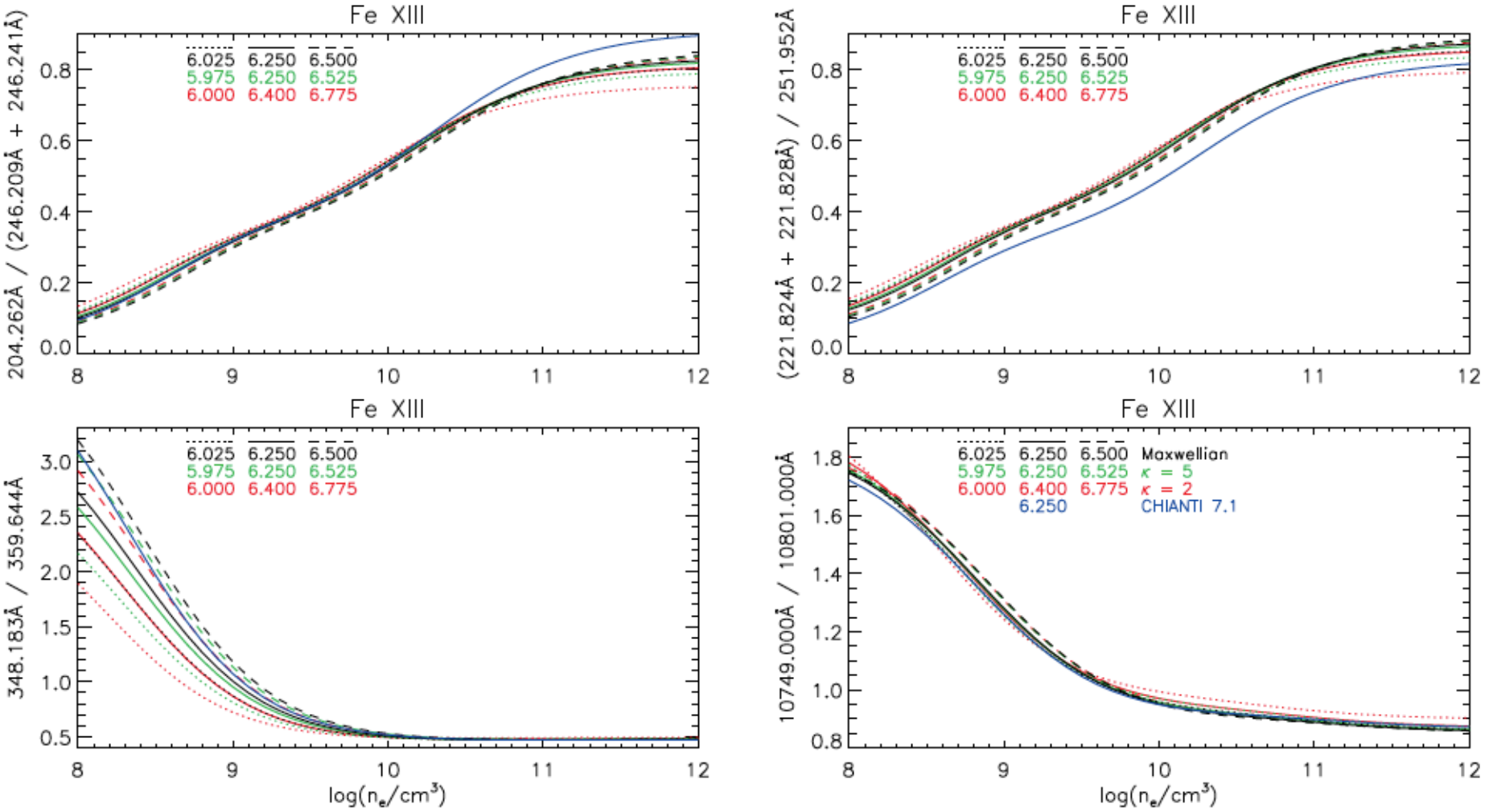
Fe XIII
204.262Å / (246.209Å + 246.241Å)
6.025 6.250 6.500
5.975 6.250 6.525
6.000 6.400 6.775
Fe XIII
(221.824Å + 221.828Å) / 251.952Å
Fe XIII
348.183Å / 359.644Å
log(n_e/cm^3)
Fe XIII
10749.000Å / 10801.000Å
Maxwellian
κ = 5
κ = 2
CHIANTI 7.1
log(n_e/cm^3)

EIS calibration (Del Zanna 2013)

The EIS SW and LW sensitivities at the start of the mission were somewhat lower than the values measured on the ground

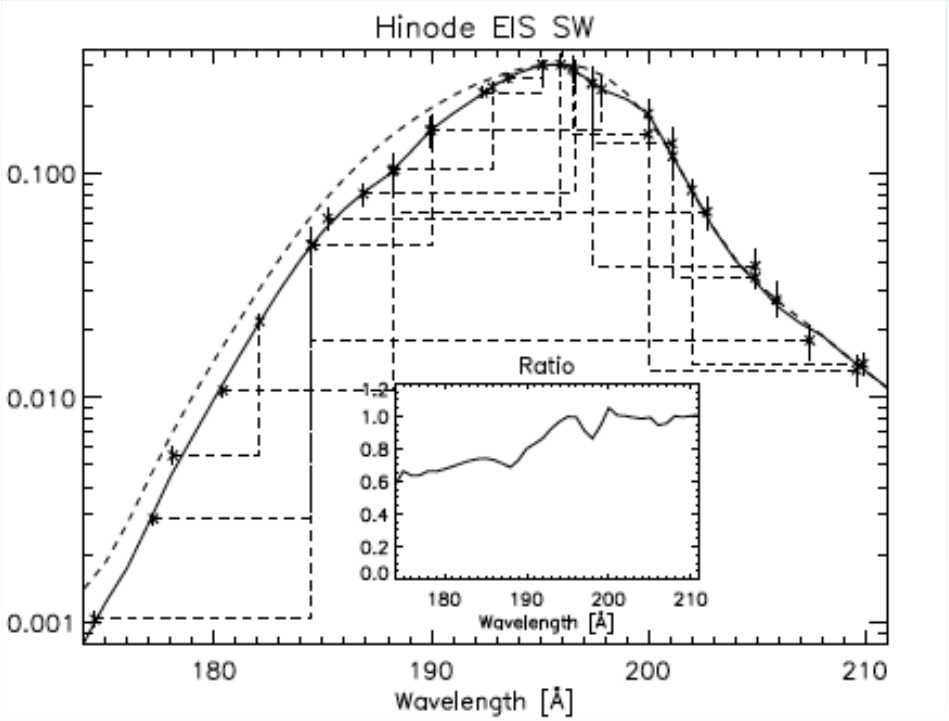

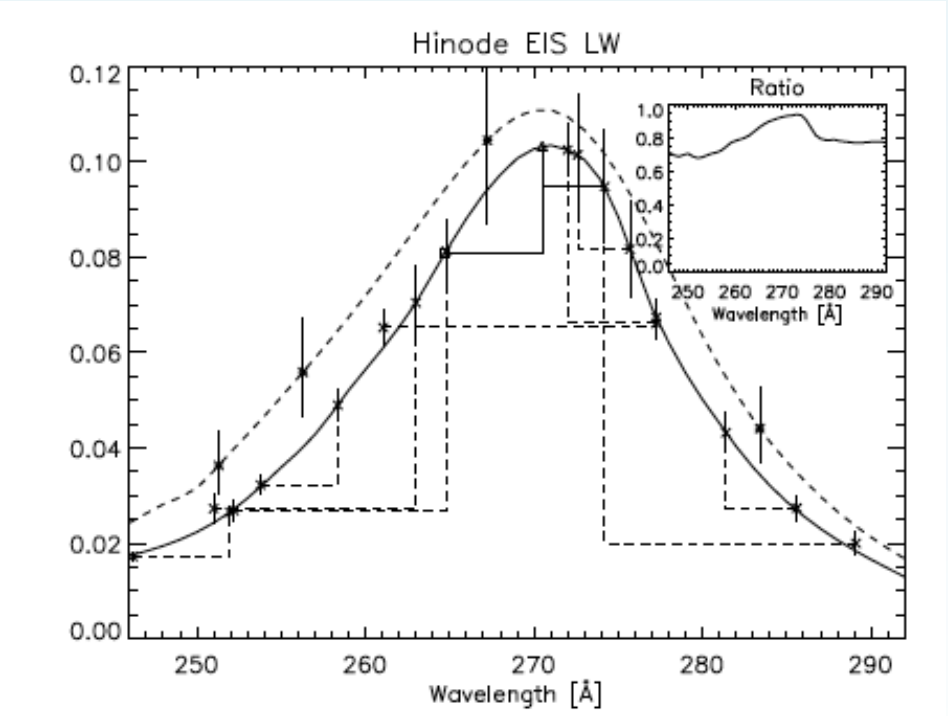

EIS and AIA calibration (Del Zanna 2013a,b)

The EIS LW sensitivity has been decreasing over time, about a factor of 2 lower by 2010 (see also Warren et al. 2013).
It was already different at the start of the mission.
Cross-calibration between AIA, EVE v.3 and new EIS shows excellent agreement (NO fudge factors for AIA)